RSC Advances

PAPER

View Article Online
View Journal | View Issue

Cite this: *RSC Adv.*, 2022, **12**, 29300

Designing dibenzosilole core based, $A_2-\pi-A_1-\pi-D-\pi-A_1-\pi-A_2$ type donor molecules for promising photovoltaic parameters in organic photovoltaic cells

Saima Rani,[a] Nabil Al-Zaqri, *[b] Javed Iqbal, *[af] Sahar Javaid Akram,[a] Ahmed Boshaala,[cd] Rana Farhat Mehmood,[e] Muhammad Umar Saeed,[a] Ehsan Ullah Rashid[a] and Rasheed Ahmad Khera *[a]

In this research work, four new molecules from the π–A–π–D–π–A–π type reference molecule "DBS-2PP", were designed for their potential application in organic solar cells by adding peripheral A_2 acceptors to the reference. Under density functional theory, a comprehensive theoretical investigation was conducted to examine the structural geometries, along with the optical and photovoltaic parameters; comprising frontier molecular orbitals, density of states, light-harvesting effectiveness, excitation, binding, and reorganizational energies, molar absorption coefficient, dipole moment, as well as transition density matrix of all the molecules under study. In addition, some photo-voltaic characteristics (open circuit photo-voltage and fill factor) were also studied for these molecules. Although all the developed compounds (**D1–D4**) surpassed the reference molecule in the attributes mentioned above, **D4** proved to be the best. **D4** possessed the narrowest band-gap, as well as the highest absorption maxima and dipole moment of all the molecules in both the evaluated phases. Moreover, with $PC_{61}BM$ as the acceptor, **D4** showed the maximum V_{OC} and FF values. Furthermore, while **D3** had the greatest hole mobility owing to its lowest value of hole reorganization energy, **D4** exhibited the maximum electron mobility due to its lowermost value of electron reorganization energy. Overall, all the chromophores proposed in this study showed outstanding structural, optical, and photovoltaic features. Considering this, organic solar cell fabrication can be improved by using these newly derived donors at the donor–acceptor interfaces.

Received 20th September 2022
Accepted 2nd October 2022

DOI: 10.1039/d2ra05934g

rsc.li/rsc-advances

1. Introduction

Despite generating more than 80% of the world's energy, non-renewable resources produce large amounts of CO_2 and have antagonistic impacts on the environment.[1] In addition, these resources are rapidly depleting over time, so the world is turning towards clean and renewable sources of energy.[2] In this regard, solar energy seems to be quite abundant, cheap, carbon-free, and safe for the environment. Furthermore, solar panels are easy to install and can function in remote areas where it is very challenging to provide electricity using other approaches. With a lifespan of more than 20 years, they demand little maintenance and require no additional land space, because of their effective installation on the roofs of homes, schools, or any other building. Consequently, they can be a good substitute for conventional electricity sources, which are overpriced and difficult to install in distant areas.[3,4] The fundamental component of a solar panel is the solar cell, which works on the idea of the photovoltaic effect. So, when photons with specific energy are absorbed by a semiconducting material, holes–electrons form and flow toward opposing electrodes to produce an electric current.[5–7] In the solar cells of the early stages, these semiconducting materials were limited to inorganic silicon ones, which despite giving good efficiencies, had constrained applications owing to their inflexible design, low competence as well as high fabricating cost.[8,9] Thus, researchers have focused their efforts on developing solar materials that are more efficient and reliable than silicon ones.[10]

[a]*Department of Chemistry, University of Agriculture, Faisalabad 38000, Pakistan. E-mail: rasheedahmadkhera@yahoo.com; rasheed.ahmad.khera@uaf.edu.pk; javedkhattak79@gmail.com; Javed.iqbal@uaf.edu.pk*

[b]*Department of Chemistry, College of Science, King Saud University, P.O. Box 2455, Riyadh 11451, Saudi Arabia. E-mail: nalzaqri@ksu.edu.sa*

[c]*Research Centre, Manchester Salt & Catalysis, Unit C, 88-90 Chorlton Rd, M15 4AN Manchester, UK*

[d]*Libyan Authority for Scientific Research, P. O. Box 80045, Tripoli, Libya*

[e]*Department of Chemistry, Division of Science and Technology, University of Education, Township, Lahore 54770, Pakistan*

[f]*Department of Chemistry, College of Science, University of Bahrain, Zallaq, Bahrain*

Recently organic photovoltaics (OPVs) have gained considerable interest as a possible alternative to silicon-based materials. These OPVs are considered more attractive because of their varied and tunable energy levels, adjustable morphology, as well as excellent purity.[11] The active layer of OPVs, responsible for the current generation by light absorption, comprises donor and acceptor materials either separated or in a bulk-heterojunction (BHJ). Between these two, the bulk-heterojunction (active layer made up by blending donor and acceptor materials) proves to be exceptional in terms of boosting the efficiencies of OPVs. Additionally, due to its tunable organic materials, the efficiencies of BHJ-based OPVs can be further enhanced by experimenting with different blends of donors and acceptors.

Between the small molecule and polymer-based donor materials, the former are preferred for bulk-heterojunctions in the fabrication of OPVs. This could be because they have a well-defined structure, are easier to purify, and also exhibit improved batch-to-batch reproducibility.[12,13] Effective device manufacturing, as well as the utilization of novel small molecule donor (SMD) materials, is credited to have achieved PCEs of up to 11 percent when fullerene acceptor molecules such as $PC_{61}BM$

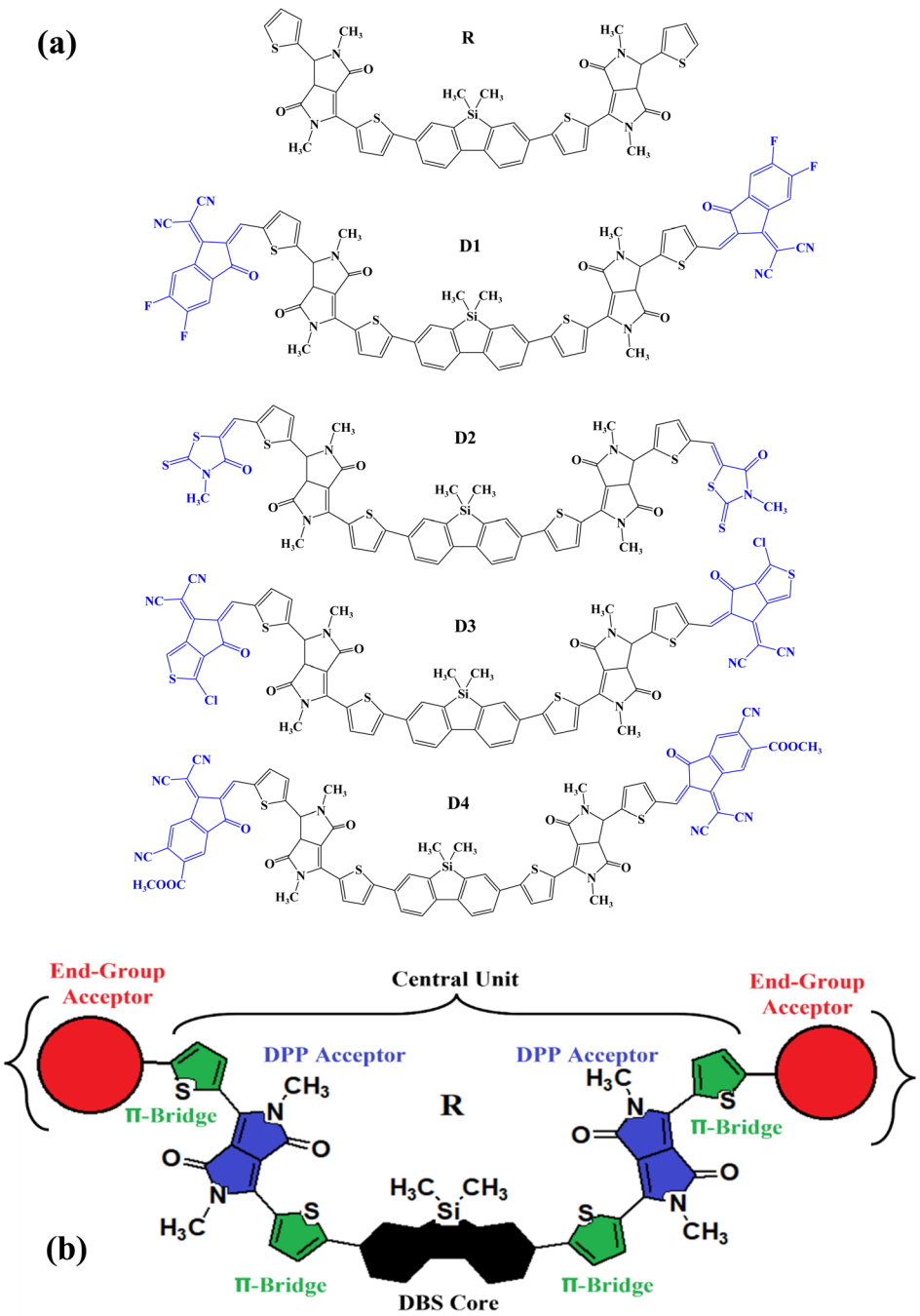

Fig. 1 (a) ChemDraw sketches of R and D1–D4 molecules, (b) molecular map of the designing strategy.

and $PC_{71}BM$ are blended with them.[14] In addition, a variety of remodeling techniques, including end-capped engineering, central core remodeling, and pi-bridge placement or substitution, can be used on SMDs to improve their various photovoltaic properties. End-capped engineering, when compared to other approaches, has several advantages. For instance, by only adding small end-capped acceptors to a molecule, the consequent morphology of the whole blend can be impacted, which as a result affects the light absorption ranges, energy levels of frontier molecular orbitals, pi-bond conjugation, and the mobilities of charge carriers, all of which have a major influence on the overall performance of OPVs. So in this research work, with the aforementioned capabilities of end-capped modification in mind, DBS-2DPP is taken as the reference molecule (**R**) and different side-chained acceptors are attached to its peripheral thiophene moieties.

DBS-2DPP is a dibenzosilole (DBS) core-based acceptor molecule with diketopyrrolopyrrole (DPP) arms attached to the DBS core *via* thiophene bridges, which are further attached to a second set of thiophene rings on each peripheral end, as shown in Fig. 1. The DBS core contains a silole moiety fused attached to two six-membered rings, and demonstrates considerable planarity and proficient charge transfer properties, whereas the DPP fragments are known to exhibit remarkable electron withdrawing properties. Collectively, the DBS-2DPP molecule shows good thermal stability and open circuit photo-voltage, voltage, along with an optical band-gap of 1.83 eV in thin film. But, when blended with a P3HT donor molecule to investigate its capabilities in OPVs, this molecule showed a photo-conversion efficiency (PCE) of only 2.05%, which might be due to its lower charge mobility, larger band-gap, and smaller absorption range.[15–17] As a result, by modifying its morphology through the addition of strongly electron-withdrawing acceptor groups at the thiophene fringes of this molecule, four new molecules (**D1–D4**) have been reported, which due to their better opto-electronic properties and smaller band-gaps prove themselves to be better than the DBS-2PP (**R**) molecule, and thus could exhibit increased PCE if taken as donors and blended with some prominent electron acceptor molecule, such as $PC_{61}BM$.

Precisely, in the formulation of the newly reported molecules, the hydrogen of the carbon closest to the sulphur of the terminal thiophene rings of the **R** molecule has been substituted with a strong electron accepting group. The reason behind the selection of this position is its reported strong electron transferring capabilities due to its seemingly planar orientation and low steric hindrance with the rest of the molecule.[18] In **D1**, the newly attached acceptor moiety was; 2-(2-ethylidene-5,6-difluoro-3-oxo-indan-1-ylidene)-malononitrile, in **D2** it was; 5-ethylidene-3-methyl-2-thioxo-thiazolidin-4-one, in **D3**; 2-(1-chloro-5-ethylidene-6-oxo-5,6-dihydro-cyclopenta [*c*] thiophen-4-ylidene)-malononitrile, while in **D4** this moiety was 6-cyano-1-dicyanomethylene-2-ethylidene-3-oxo-indan-5-carboxylic acid methyl ester. Chemdraw sketches of reference **R** and **D1–D4** chromophores are given in Fig. 1(a).

2. Computational details

To explore various optoelectronic properties of the studied structures, a quantum mechanical technique based on density functional theory (DFT) was employed with the help of Gaussian 09 software.[19] In order to avoid excessive computational cost, the long alkyl side chains of DBS-2DPP (taken as **R** in this work) were replaced with methyl groups based on their general inconsequential influence on the optical and electronic attributes of the overall molecule.[20] GaussView 6.0 (ref. 21) was employed to draw the structures of **R** and **D1–D4** molecules and to visualize various outputs as well.

Firstly the **R** molecule was subjected to four different exchange-correlation functionals of DFT, *i.e.*, B3LYP,[22] CAM-B3LYP,[23] MPW1PW91,[24] and ωB97XD[25] at 6-31G (d, p) basis set to attain any one functional with the best imitation of the experimental work.[26] So, the maximum absorption wavelengths (λ_{max}) of all the afore-stated functionals were compared to the experimental value of **R**. And for this reason, time dependent DFT was exercised to obtain the UV-Visible profile of **R** under solvent phase with these functionals. It should be noted that in the cited literature the absorption spectra of **R** were calculated using dichloromethane solvent, thus the very same environment of solvent was applied to the molecules of this study using the integral equation formalism variant of the polarizable continuum model (IEFPCM).[27] As shown in the graph of absorption attained with the aid of Origin 6.0,[28] the maximum absorption wavelength (592 nm) produced by the B3LYP functional is consistent with the published value (596 nm) of **R** (Fig. 2), while that of the other three functionals were too far off to be of consequence, as CAMB3LYP showed a λ_{max} of 4845 nm, MPW1PW91 565 nm, and ωB97XD had its value of 471 nm. Subsequently, B3LYP functional with 6-31G (d, p) basis set was selected for further calculations of **R** and devised compounds.

After the selection of the desired functional, the molecules were optimized at their ground state to understand their geometry. For this purpose, the bond length and dihedral angle

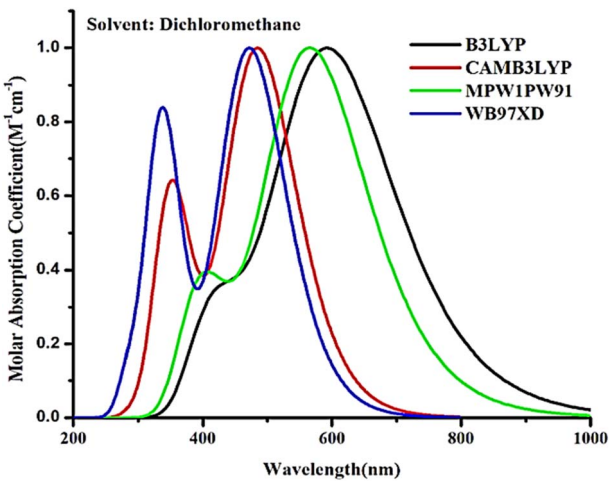

Fig. 2 Absorption profile of R (DBS-2DPP) calculated by using four hybrid functionals in dichloromethane solvent.

of the carbon–carbon bond between the thiophene ring and the newly added acceptor group at their site of attachment were studied. To validate the geometry of the molecules, span of deviation from plane (SDP) and molecule planarity parameter (MPP) were also explored. These two parameters, in addition to, the transition density matrix (TDM) of all the examined molecules were created using the Multiwfn program,[29,30] while VMD 1.9.3 (ref. 31) was utilized to visualize MPP and SDP. Furthermore, the frontier molecular orbitals (FMOs) were also generated at the ground state to visualize the wave-function of the highest occupied (HOMO) and the lowest unoccupied (LUMO) molecular orbitals, and from these FMOs, the band-gap was also calculated. In addition, the graphs of density of states (DOS) were plotted with the help of PyMOlyze 1.1 (ref. 32) to investigate the electronic densities at various energy levels and also to authenticate the FMOs' findings.[33]

At the excited state, the excitation energies, absorption maxima, dipole moment, oscillator strength, transition density matrix, binding energies, *etc.* were investigated to attain the optoelectronic attributes of the molecules after absorption of light. Similarly, the fill factor, light harvesting efficiencies, and open circuit photo-voltage were computed to scrutinize the photovoltaic properties of the molecules and to give a direction about their photovoltaic efficiencies.

Lastly, the internal reorganization energies of the explored molecules were also computed with the help of their optimized neutral, anionic, and cationic states. Thus, the following eqn (1) and (2), taken from Marcus theory, were used to compute the two components of internal reorganization energies, *i.e.*, for electrons and holes, respectively.[34]

$$\lambda_e = [E_0^- - E_-] + [E_-^0 - E_0] \quad (1)$$

$$\lambda_h = [E_0^+ - E_+] + [E_+^0 - E_0] \quad (2)$$

Optimized anionic and cationic geometries were used to compute molecular neutral energies E_-^0 and E_+^0 respectively. E_0^+ and E_0^- are the single point energies of cations and anions at ground level, estimated by employing optimized neutral molecule geometries. E_- along with E_+ are the energies of anion and cation calculated using neutral molecule's anion and cation structural optimization. Finally, E_0 demonstrates the neutral molecule's ground state energy.

3. Results and discussion

3.1. Ground state geometries and planarity measurements

Optimized structures of **R** and modified chromophores (**D1–D4**) at their ground state, computed through B3LYP functional, are presented in Fig. 3. From these optimized geometries, the planarity in the molecules was estimated to be quite substantial, which could be attributed to the two smaller thiophene entities present between the large acceptor and donor groups of the molecules. These thiophene rings, by acting as bridge between the acceptor and donor entities, reduced the overall steric hindrance within the molecule and increased the planarity, which as result, enhanced the conjugation in the molecules under scrutiny. To quantitatively understand the planarity and conjugation of the newly added acceptors with respect to the rest of the molecule, the dihedral angles and bond length values were obtained at their point of attachment with the thiophene ring of the molecule.

It was discovered that the studied bond length of all the newly reported compounds fell at 1.42 Å, indicating significant conjugation and charge transfer between the molecule and the newly added acceptors. This conjugation was evaluated with the fact that the range of a carbon–carbon bond to have conjugation in it is between the single bond (C–C; 1.54 Å) and double bond (C=C; 1.34 Å) lengths. The closer a C–C bond is to the double bond length, the greater could be its conjugation. Furthermore, in **D1–D4**, the measured dihedral angles ranged from 0.21° to 2.97°,[35] as shown in Table 1. These low values of dihedral angles illustrated the planarity of the molecule at this bond.

But to evaluate the overall planarity of these compounds and to compare it to that of the reference molecule, the molecular planarity parameter (MPP) and the span of deviation from the plane (SDP) values were computed (Fig. 3). Here, it is known that the structure will be more planer if it has smaller values of both MPP and SDP. So, the lower MPP (0.304 Å) value indicates that the reference (**R**), *i.e.*, the central region, except for the added acceptors, has quite a planer structure, which is also indicated by its SDP (1.196 Å) results. Whereas, amongst the designed compounds the maximum deviation from planarity has been observed by **D4**, which may be due to the steric hindrance caused by its bulky end-groups, which rendered the molecule slightly non-planer as compared to other structures. Correspondingly, **D1**, **D2**, and **D3** also showed slight deviation from the plane, again attributed to their added end-groups. In Fig. 3, the deviations of these structures from the plane are shown in pictorial forms. Where the red color shows those areas, which are below the plane of paper, while the blue color areas are those which are above the plane of paper. This coloring scheme gives a very good idea about the different parts of these molecules, which deviate from the fitting plane. In **R** molecule, it is observable that there are a few blue and red parts at the DBS core and a few of them are also present at DPP acceptors, but the overall structure is quite planer.

But, in **D1** molecule, there are very light red and blue hues on the central and right part of this molecule, which indicate planarity, but a little deviation occurs at the end-group on the left side. Similar deviation from the plane has been observed in the case of other the three derived molecules, in which the whole structure is quite planer, but deviations are observed in right end group of **D2** and **D4**, as well as left end group of **D3**, resulting in the slight deviation of their structures from the plane.

Though the values of these two parameters, *i.e.*, MPP and SDP of the four modified molecules are comparatively higher than the reference molecule, still their rather low values certify their planarity. Also, it should be noted that this slight deviation of the planarity of the reported molecules, could be supportive in case of their charge density dispersal. As molecules with high values of planarity tend to have a rather dispersed charge density, like the FMOs of the reference molecule (Fig. 6). While

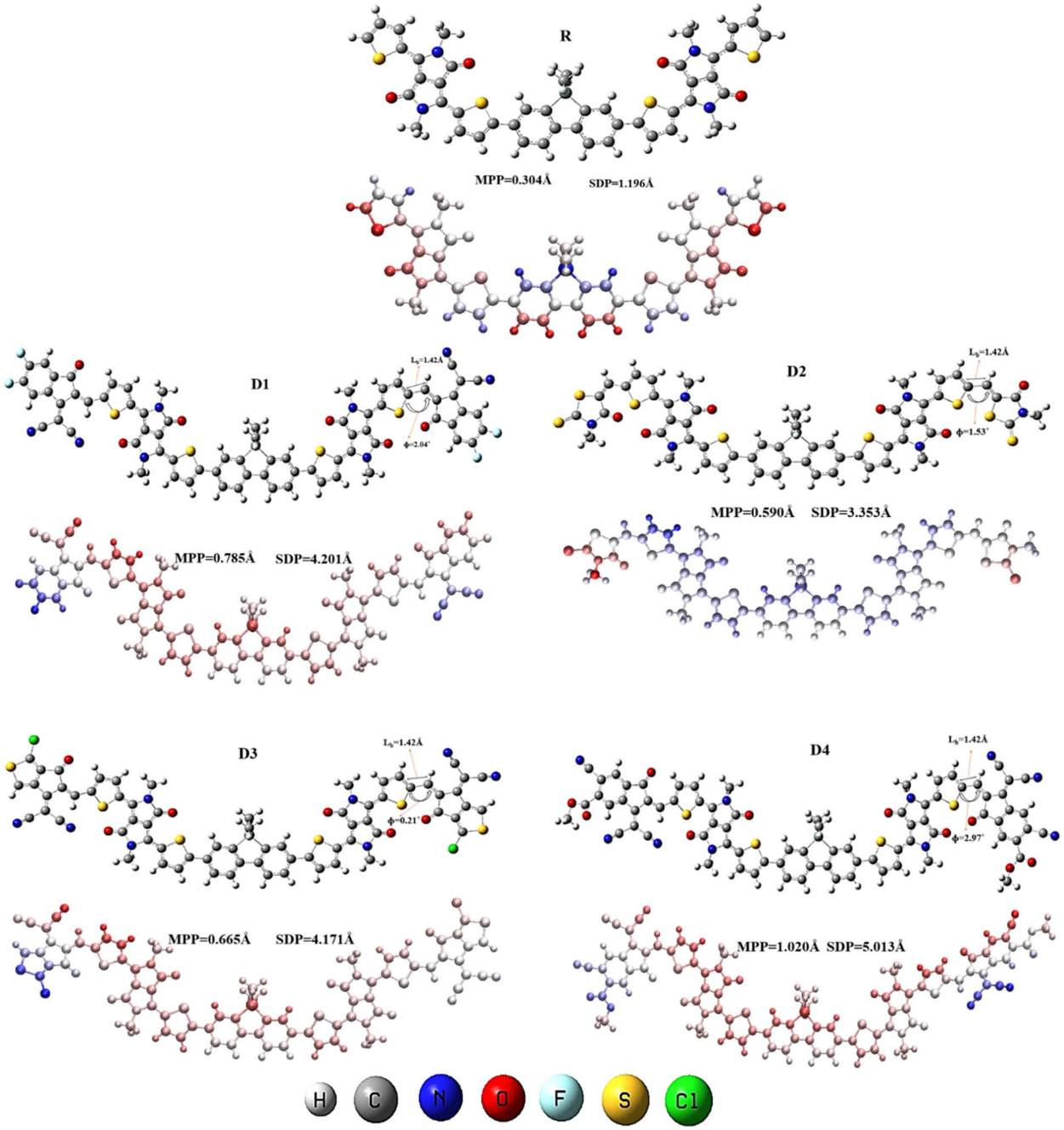

Fig. 3 Optimized structures (along with the studied bond parameters of the designed molecules), the molecular planarity parameter (MPP), the span of deviation from the plane (SDP) of **R** and **D1–D4**.

Table 1 Bond lengths (Å), dihedral angles (θ°), the molecular planarity parameter (MPP) (Å), and the span of deviation from the plane (SDP) (Å) for **R** along with newly developed **D1–D4** small chromophores

Molecules	Bond length (L_b) (Å)	Dihedral angle (Φ) (θ°)	Molecular planarity parameter (MPP) (Å)	Span of deviation from plane (SDP) (Å)
R	—	—	0.304	1.196
D1	1.42	2.04	0.785	4.201
D2	1.42	1.53	0.590	3.353
D3	1.42	0.21	0.665	4.171
D4	1.42	2.97	1.020	5.013

the designed molecules due to their deviation from planarity have retained the charge densities of their FMOs in such a way that it could be helpful in charge transfer from the HOMO towards the LUMO.

3.2. Optical parameters

The optical properties of studied molecular structures were investigated in order to evaluate the light harvesting efficiency (LHE) and performance of the organic solar systems of the corresponding molecule.[36,37] A combination of the TD-DFT and the selected functional was used to determine the spectral and photo-physical properties of the newly constructed structures (**D1–D4**) along with **R** (reference molecule) in both the solvent (dichloromethane-DCM) and gaseous medium.[38] The values of the computationally determined optical parameters, *i.e.*, the absorption range, absorption maxima (λ_{max}), excitation energy, oscillating power, and transition coefficient for each of the four designed molecules **D1–D4** and **R** (reference), are provided in Tables 2 and 3.

Interestingly, all of the newly formulated compounds exhibited a bathochromic shift in their absorbance maxima, supporting our claim that the added peripheral acceptor groups have increased the conjugation and, by association, the electron transfer within the new molecules. In addition, the presence of the DCM solvent has enhanced the absorption profile of the molecules formulated in this study. Consequently, the absorption spectra (Fig. 4) indicates that dichloromethane shifted the absorption peaks of the electromagnetic spectrum in the higher visible region for **D2** and near infrared regions for other newly created molecules. Precisely in the studied solvent, **R** has a maximum wavelength of 592 nm, while the maximum absorption wavelengths of the newly reported compounds (**D1–D4**) are 840, 744, 858, and 876 nm, respectively. Similarly, in the gas medium, the order of absorption maxima followed by the studied molecules is the same as of DCM solvent; **D4** > **D3** > **D1** > **D2** > **R**. Furthermore, the absorption range of **R** in both the phases is narrower as compared to the broad ranges of all the newly formulated **D1–D4**. These results imply that the newly created compounds under research have a better absorption profile as compared to **R** molecule. Individually, because of the presence of the unsaturated acetyle and cyano groups in the acceptor unit in **D4**, it has the maximum absorption value of 876 nm and 802 nm in the solvent and gaseous medium, respectively. This implied that **D4** might also have the lowest band-gap energy among all, solidifying its candidature in efficient photovoltaic devices. The reason behind this assumption is that generally, molecules with high absorption peaks tend to have lower band-gap, for easier transfer of electrons between the FMOs upon absorption of photons.[39]

One of the properties related to photo-absorption is excitation, which occurs when a low-energy state electron is stimulated electrically to a high-energy state. Effective electron transport, along with greater spectral absorption at a longer wavelength may be accomplished, as a consequence of a smaller energy difference between the two states in which the excitation is to occur.[40] This energy difference could be attributed to the energy needed for excitation, *i.e.*, excitation energy, a significant optical feature.[41] According to the results tabulated in Tables 2 and 3 for the first excitation energy values, *i.e.*, between the FMOs, all of the newly developed molecules had lower excitation energies than reference, suggesting that the electron transport process between their molecular orbitals (HOMO and LUMO) might be more accelerated than reference. Actually, the effective electron-withdrawing newly added acceptors of the designed molecules increase the possibility of electronic excitation and thus lowers the required excitation energy.

Table 2 Absorption values (λ_{max}), excitation energy E_x (eV), oscillation strength (f_{os}), light-harvesting efficiency (LHE), molecular state, as well as percentage transition character of (D1–D4) designed and R molecules in the dichloromethane solvent medium

Molecules	Calculated λ_{max} (nm)	Experimental λ_{max} (nm)	E_x (eV)	f_{os}	LHE	Molecular states	Transition character
R	592	596	1.98	1.23	0.940	$S_0 \rightarrow S_1$	70%
D1	840	—	1.42	1.97	0.989	$S_0 \rightarrow S_1$	67%
D2	744	—	1.62	1.95	0.988	$S_0 \rightarrow S_1$	67%
D3	858	—	1.40	2.02	0.990	$S_0 \rightarrow S_1$	66%
D4	876	—	1.36	1.84	0.985	$S_0 \rightarrow S_1$	68%

Table 3 Absorption values (λ_{max}), excitation energy (E_x), oscillation strength (f_{os}), light-harvesting efficiency, molecular state as well as percentage transition character of (D1–D4) designed molecules and R in the gaseous phase

Molecules	Calculated λ_{max} (nm)	E_x (eV)	f_{os}	LHE	Molecular states	Transition character
R	578	2.02	1.00	0.901	$S_0 \rightarrow S_1$	70%
D1	781	1.51	1.63	0.976	$S_0 \rightarrow S_1$	68%
D2	702	1.69	1.60	0.974	$S_0 \rightarrow S_1$	68%
D3	794	1.48	1.65	0.977	$S_0 \rightarrow S_1$	68%
D4	802	1.47	1.62	0.976	$S_0 \rightarrow S_1$	68%

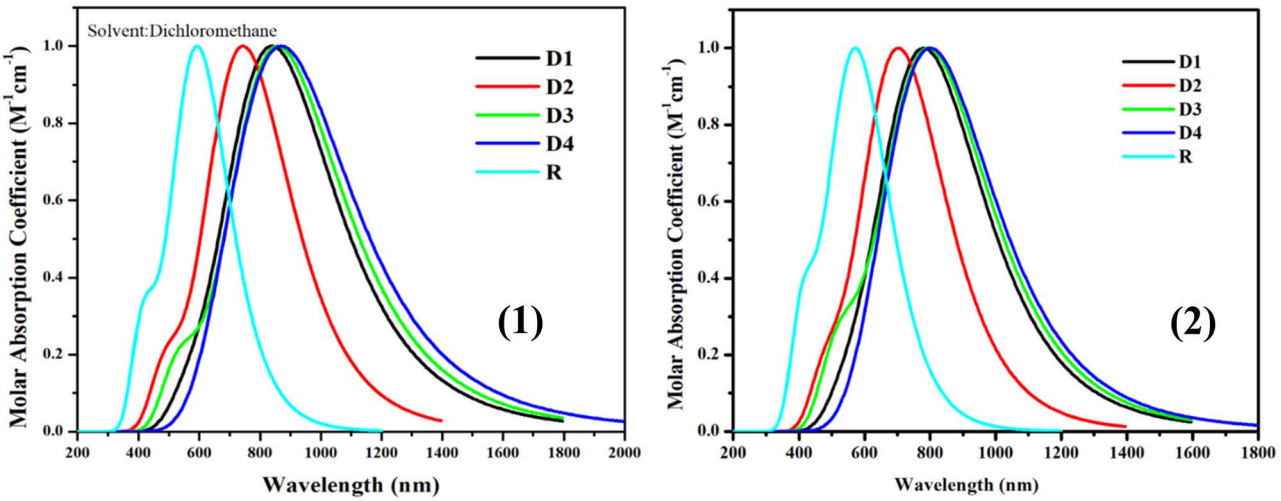

Fig. 4 UV-Vis spectra of scrutinized D1–D4 along with R in the (1) solvent phase (dichloromethane) and (2) in gaseous medium.

The oscillation strength is generally used to compute the statistical probability of an electronic transition from the initial ground level to an excited level (first in our case) after light absorption by the molecule. It has been shown in literature that strong acceptor moieties are responsible for the higher oscillation strength of any molecule.[42] The oscillator strength values in Tables 2 and 3 of optical properties, illustrates the higher oscillation strengths of the derived molecules as opposed to the reference. Here, the studied molecules followed the increasing order of **R** < **D4** < **D2** < **D1** < **D3** in the solvent medium and of **R** < **D2** < **D4** < **D1** < **D3** in the gas medium. The highest oscillation strength of **D3** in both mediums demonstrates its high aptitude for utilization in organic photovoltaics. In addition, to determine the probability of electronic transition of an electron between orbitals of study, oscillation strength plays a momentous role in calculating the light harvesting efficiencies of a molecule, the values for which are also tabulated in Tables 2 and 3

3.3. Light harvesting efficiency (LHE)

LHE of solar materials is used to assess the optical qualities, J_{SC}, and efficacy of the cell, as it estimates the production of the charges produced after the absorption of incoming photons.[43] It is directly dependent on oscillation strength and is determined by given eqn (3).

$$\mathrm{LHE} = 1 - 10^{-f} \quad (3)$$

where f specifies the oscillator strength and LHE; the evaluated light harvesting efficiency. In comparison to **R**, all new compounds were shown to have superior LHE values because of their greater values of oscillator strengths.

Among all the newly tailored structures, **D3** had the highest LHE because of the highest overlapping of pi-orbitals in combination with the lowest dihedral angle between its added peripheral and core of the molecule, which permits a more efficient electronic transition.[38] It is clear from the values of light harvesting efficiency that the newly added acceptors at the peripheries of the molecules have directed the transfer of charges towards themselves and enhanced the conjugation, which benefited the molecule in harvesting light effectively and transporting the thus generated charges within itself. Thus, as opposed to the reference molecule, all newly created compounds could be taken into consideration as conspicuous small molecules donors in organic photo-active layers of photovoltaic cells. Till now, amongst all the newly developed molecular structures, **D4** with its lowest excitation energy and highest absorption maxima, along with **D3** with its second highest absorption maxima, and highest oscillator strength, and by association, highest LHE seems to be the most effective organic chromophores for their exploitation in OPVs.

3.4. Quantum mechanical descriptors [HOMO and LUMO]

FMOs (Frontier molecular orbitals) of a molecule can be described as; LUMO-the lowest unoccupied molecular orbital and HOMO-the highest occupied molecular orbital. When

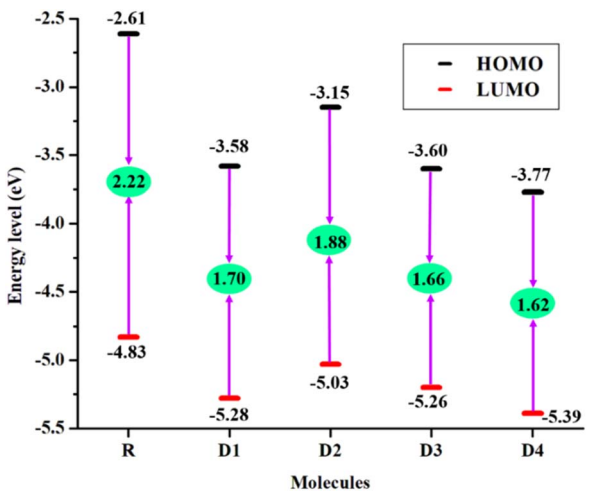

Fig. 5 Band-gap plot of R along with D1–D4 designed chromophores.

characterizing the optical characteristics of a molecule, FMOs' quantum mechanical analysis reveals the presence of HOMO–LUMO's electronic distribution patterns in the molecular electronic structures.[44,45] The electronic distribution of FMOs has been utilized to anticipate the intramolecular charge transfer (ICT), during which the electron density moves from the ground state's valence band (HOMO) to the excited state's conduction band (LUMO). From Fig. 6, it is distinctive that in the reference molecule, electron density is uniformly distributed throughout the structure in both the studied FMOs. This diffusion of electronic density over the whole molecule could be due to the highly planar geometry of the molecule, as evaluated by the study of its MPP and SDP.

But for the efficient transfer of an electron from the valence-HOMO to the conduction-LUMO band, the most proficient approach is for the HOMO to be present around the donor region and the LUMO to be over the acceptor region. In other words, the localization of both FMOs should be at different sites. Similar is the case in the **D1–D4** structures, where the electron density of HOMO is dispersed uniformly on the DBS core, benzothiazole acceptors, and thiophene bridges, while in the LUMO state this electron density has moved towards the newly added peripheral acceptors. This peculiarity of charge density is evaluated to be because of the added dimensionality in the molecules created in this study. Also, it was noted that the charge density is present around the thiophene rings in both the FMOs, which exhibits their proficient contribution to the transfer of electrons (Fig. 6).

Overall, in the considered molecules, the order of stabilization for HOMOs is **D4** > **D1** > **D3** > **D2** > **R**, while the order in which LUMO energies are most stable is as follows: **D4** > **D3** > **D1** > **D2** > **R**, as seen in the graph of band-gap in Fig. 5. Values computed for

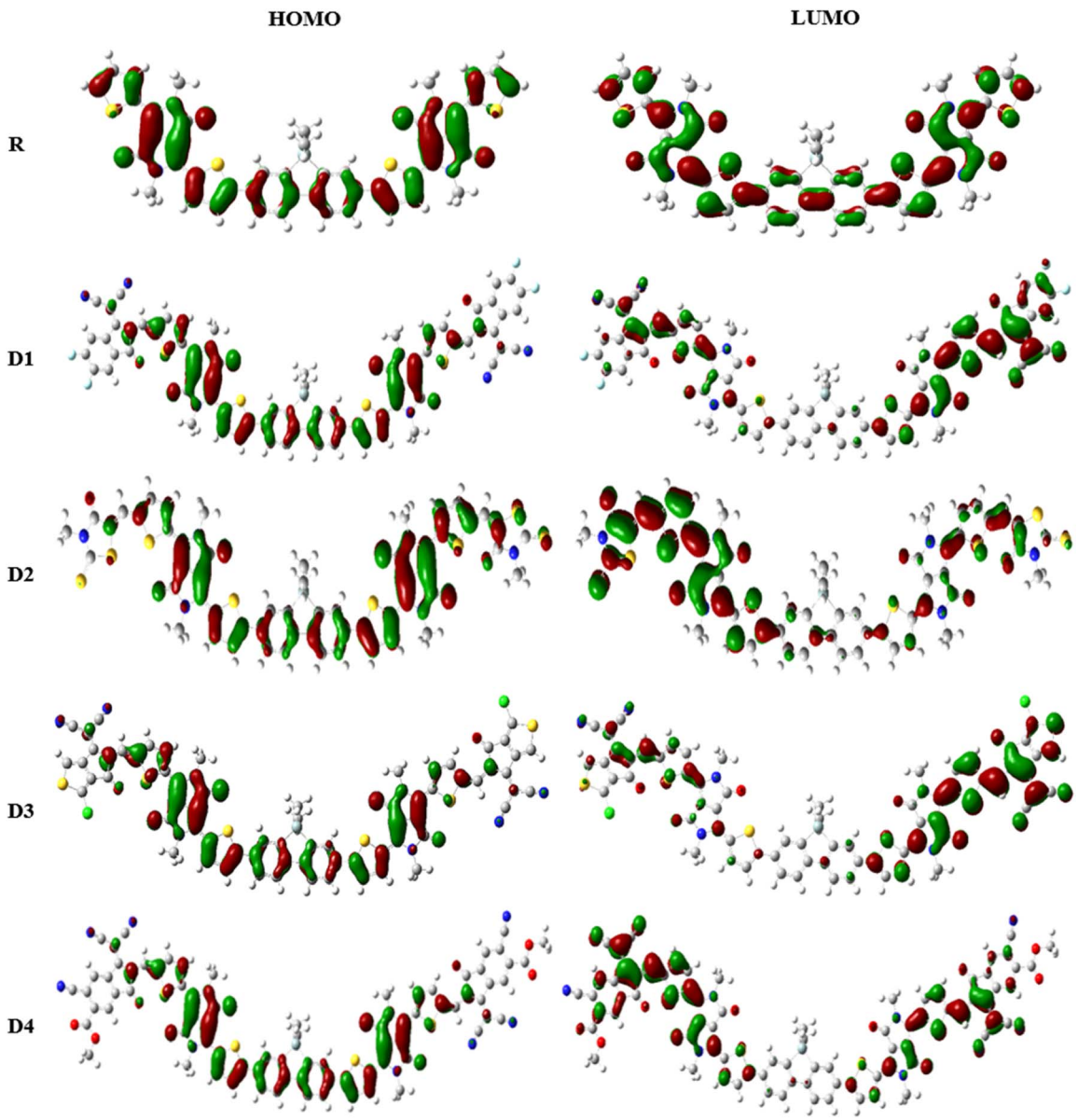

Fig. 6 HOMO–LUMO charge density dispersal of R and newly formulated small molecules D1–D4 at their optimized geometries.

FMOs in Fig. 5 indicate that the HOMO of **D1–D4** exhibits greater stability and contains lower energy as compared to the **R**'s HOMO. This greater stability is attributed to the added electron withdrawing acceptor groups in the derived molecules. Amongst all, the largest electron withdrawing acceptor group of **D4** molecule with its prolonged conjugation has triggered this molecule to be the one with the most stability, which might also help it in being a proficient donor at the photo-active layer. In addition, the most significant charge separation is also present in the LUMO of this molecule, which could be attributed to its highest values of the evaluated planarity parameters.

Usually, the greater the capability of an electron withdrawing group to extract the electrons from the donor region, the decreased will be value of the HOMO and LUMO energies.[46] The band-gap, between the energy values of the FMOs, is closely related to the absorption maxima, as molecules with a lower band-gap tend to have a higher value of this important parameter. In addition, a lower band-gap increases the reactivity and also the charge transfer within the molecule. This band-gap is the energy difference between the evaluated valence and conduction bands of a molecule. From Fig. 5 it's perceived that the reference molecule possessed an E_g of 2.22 eV, while the E_g of **D1–D4** molecules were much smaller when compared with **R** molecule. The order of band gap of the molecules of this study is **R** (DBS-2DPP) > **D2** > **D1** > **D3** > **D4**. The reason behind these lowered values of band-gap of the newly modified molecules is the added peripheral acceptor groups, which by enhancing the conjugation have reduced the values of the band-gap, and thus made the transfer of electrons between the FMOs much easier. Though all the newly created molecules have a low band-gap, **D4** has the lowest band-gap of all because of its most stable and differentiated FMOs and strongly conjugated end-capped electron acceptors containing cyano and acetyl groups. So, we could assume that amongst all the molecules under study, **D4** might be the best possible candidate for possible future applications in organic photovoltaics, with **D3** being a close second.

3.5. Density of state (DOS)

DOS offers specific information about the availability of charges in different energy levels along with their possible electronic excitation.[45] In the plots of DOS, both the partial (PDOS) and total (TDOS) graphs are provided for a proper understanding of each fragment's contribution to total DOS (Fig. 7). Through the plots of density of states at the selected functional, plotted through PyMOlyze 1.1, further investigation to infer the validity of results drawn from FMOs was made possible. The relative intensity in the DOS graphs is represented at the vertical axis, whereas energy, (measured in electron volts) is represented at the horizontal axis. The graphs essentially depict the number of electronic states present, at a specific energy level and the contribution of a specific fragment in the elevation of that energy level.[47] In regards to the FMOs, the planar zone in these plots, having no peak, depicts the band-gap, while the first peak towards its left represents the HOMO and that towards the right; the LUMO, and the values for which are in agreement with the values attained from the FMOs analysis above.[48,49]

Precisely in the DOS plots, the molecules were subdivided into four portions to comprehend their probable discrete contributions to the total electron density states, these parts are referred to as the bridge, the core (donor), the acceptor 1 (or acceptor in case of reference), and the acceptor 2 (the newly added one). These plots depict the overall molecular absorption (total DOS) by magenta line, while the individual contributions (PDOS) of the fragments are shown by red, black, green, and blue lines, respectively. Because of the added acceptor groups, the newly formulated molecules have high-intensity peaks of TDOS in their conduction band (towards the right of LUMO), illustrating the enhanced probability of residence of electron in this band, *i.e.*, better electron transfer than reference. Individually, the peaks of acceptor 2 (blue) are the highest in case of **D4** molecule, attributed to its most proficient abilities till now. Similarly, the acceptor groups in all the newly formulated compounds have varying strengths and conjugation levels, making the peaks of graphs differ from each other.

The Mulliken data of all the evaluated molecules, illustrating the percentage contribution of each fragment in raising the FMOs are presented in Table 4. In case of the reference molecule, all three fragments showed somewhat equal contribution in elevating its FMOs, which could retard the probable charge transfer from the HOMO towards the LUMO in the molecule. On the other hand, upon the addition of peripheral acceptors (acceptor 2), the percentage contribution of each fragment has improved drastically. The contribution of the donor in the LUMO has reduced from a 13% (**R**) to just 2.6–5.3% in the derived compounds, which could mean that the added acceptor fragments have shifted the LUMO electronic density towards themselves. Thus, the percentage contribution of both the acceptor fragments (1 and 2) in LUMO charge density have also increased in the designed molecules as compared to the acceptor 1 of the reference. These results signify the aptitude of the newly added fragments in differentiating the HOMO and LUMO in donor and acceptor, respectively, which could enhance the transfer of charges in the molecules. On a side note, the relatively unchanged contribution of the thiophene (bridge) fragments in the FMOs of the derived molecules validates their prominent charge transfer between the core and the peripherally added acceptors.

Furthermore, the Fermi levels of the studied molecules were also calculated and are represented in Fig. 7 of the DOS spectra for each molecule. These values are the average of the FMO energy levels and represent the tendency of an electron to reside, either in the conduction band or the valence band. Here, to the left of the central planar region is the valence band and towards its right is the conduction band.[50] The more the Fermi level is towards the conduction band the greater is its tendency to be an acceptor, while the opposite is true for a molecule to show donating properties.[41]

3.6. Transition density matrix (TDM)

By using the transition density matrix; in conjunction with electron excitation predictions, delocalization and coherence length of electron and hole pairs can be predicted.

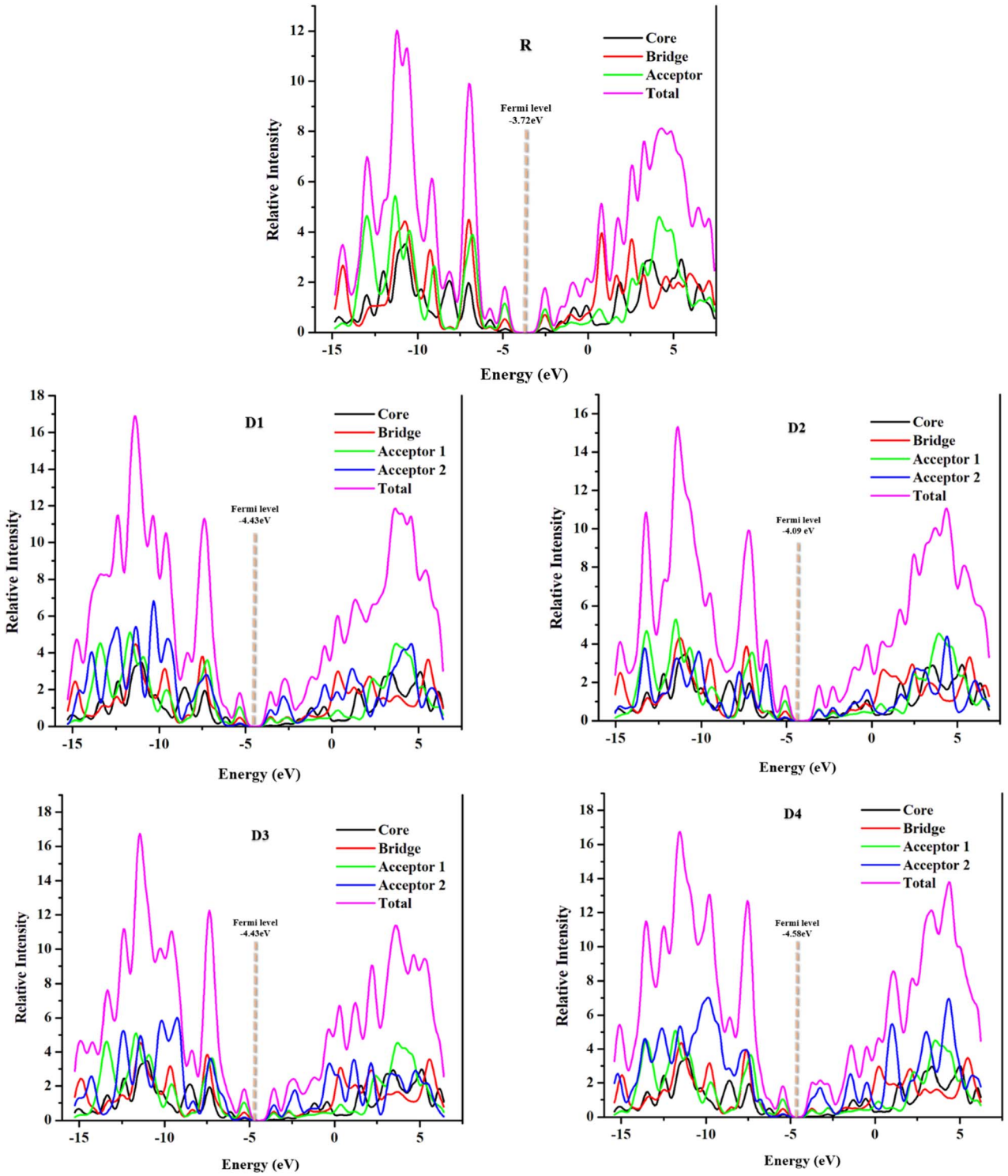

Fig. 7 DOS curve plots of D1–D4 and R.

Furthermore, the relationship among the core (donor), bridges, and acceptors can be determined by using the transition density matrix.[44,51] Precisely, during excitation, interaction among donating and receiving moieties, in addition to the quantum geometry of the overall molecule, is determined with the help of TDM.[52,53] The TDM plots are the spatial maps used to describe electronic excitation procedures in light harvesting devices like OPVs, in which electron density travels from the core to the acceptor moiety *via* pi-conjugation inside the molecules.[54] In TDM graphs of Fig. 8, hydrogen atoms were excluded and disregarded owing to their negligible share in the overall excitation. So, at B3LYP/6-31G (d,p), every molecule, except for

Table 4 Bridge (thiophene), acceptor and donor (DBS) participation in rising the HOMO & LUMO of R (DBS-2DPP) as well as architecture molecules (D1–D4)

Molecules	FMOs	Acceptor 1 (%)	Acceptor 2 (%)	Bridge (%)	Donor (%)
R	HOMO	58.5	—	30.2	11.2
	LUMO	48.5	—	38.6	13.0
D1	HOMO	52.8	8.6	26.9	11.6
	LUMO	24.5	44.7	27.8	3.0
D2	HOMO	53.0	8.9	27.7	10.4
	LUMO	34.3	27.7	32.7	5.3
D3	HOMO	52.7	9.3	26.7	11.4
	LUMO	23.9	45.7	27.5	2.9
D4	HOMO	51.9	9.4	26.7	11.9
	LUMO	21.7	50.1	25.6	2.6

reference, has been distributed into four moieties; donor (D), mid acceptors (A_1), peripheral acceptors (A_2), and bridge (B), while the reference constitutes three fragments, by excluding the A_2 fragments (Fig. 8). This differentiation of fragments was done to better describe how the electrical charge density is localized or delocalized at these moieties. Varying fragments (ranging from one to the total no. of atoms in the molecule, except hydrogen) are labelled on the bottom horizontal and left vertical axis, while the electron density of the molecule is indicated through a colored bar on the right *y*-axis of the TDM maps. Uniform charge distribution, as well as coherency, is seen in the designed molecules, attributed to their added A_2 component. Furthermore, the charge transfer is present discreetly in the diagonal and off-diagonal directions of these molecules. Overall, the donor region of all the molecules, including reference, shows a rather low charge density, while brightly colored zones in the acceptor regions of the molecules depict the high charge density in them, meaning effective charge distribution towards acceptors.

3.7. Exciton binding energy

A constructive aspect of OPVs, the binding energy (E_b), is generally exploited to make predictions regarding electrical and optical characteristics, or the overall performance of an OSC.[55] Bound charge carriers (excitons) are produced at the photoactive layer of an OPV after photon absorption by the organic chromophores. It is necessary to disintegrate the exciton into opposite charge carriers of holes and electrons, in order to make their migration towards their respective electrodes possible. As a result of the strong coulombic attractive interactions between the generated charge carriers in the organic conjugated chromophores, their dissociation into separate charges becomes difficult. In order to elevate this phenomenon of dissociation, a convenient alternative method is to lower the binding energy of the respective molecule. This binding energy could be lowered by separating the acceptor and donor components within a molecule so that the respective holes and electrons could easily travel towards either of the two portions of the molecule. In the designed chromophores, the existence of the newly added acceptor moieties has distinguished the acceptor and donor regions within the molecules effectively, making it feasible for the molecule to have lowered binding energies between the charge carriers of the excitons due to the lowered coulombic attractive forces between them. Individually, the greater the electron withdrawing capability of the added acceptor fragment, the lowered the binding energy. For this reason, the binding energy of the **D4** molecule is the lowest one of only 0.15 eV in the gas phase. Similarly, the designed chromophores in the gas medium, all have lowered binding energies than the reference, due to their prominently electron withdrawing added terminal acceptors. Overall, the declining order of exciton binding energy in the gas phase followed by all the molecules of this study is; **R** > **D1** = **D2** > **D3** > **D4**. But in the dichloromethane solvent, the trend is as; **D1** > **D2** = **D3** = **D4** > **R**. Although in the solvent medium the designed chromophores have comparatively higher binding energies than reference, these values illustrate the enhanced capability and aptitude of the derived molecules with the polar solvent studied.[33] Though the calculation of binding energy through theoretical evaluation is rather difficult, but the estimated guess is presented in this research work with the help of eqn (4). The values of the binding energies of all the molecules in both the gas medium and DCM solvent were calculated from eqn (4) and are demonstrated in Table 5.[56]

$$E_b = E_g - E_x \quad (4)$$

Here, E_x is the minimal amount of energy required in order to accomplish the first excitation from (S_0–S_1), in other words, the first excitation energy values, taken from Tables 2 and 3 While the values of the energy gap between the FMOs (E_g) are taken from Fig. 5.

3.8. Reorganizational energy (RE)

Extent of charge carrier transit characteristics is most likely to be done using reorganization energy (RE), measured in eV.[57,58] The internal and the external RE are the two forms of reorganization energies required by a molecule. Internal reorganization energy informs about the variation in internal geometry of a molecule upon charge dispersal. While "external reorganization energy" is a term used to describe the effects of the environment outside the optical system. Because external reorganization energy has less impact on our present research (due to the unchanging external environment) and also is difficult to assess, it has been disregarded here.[37]

The mobility of charges between donor, as well as acceptor components, in each molecule, is assessed using internal RE. Charge mobility rate has an inverse relation with RE values. The strength of the charge transfer between donor and acceptor units is estimated using the internal RE.[59] Specifically, when the internal reorganization energy is decreased, the value of the rate of charge mobility is projected to be increased accordingly. The likelihood of electron and hole transfer in donors and acceptors is highly dependent on the structural characteristics of the moieties involved. The studied reorganization energy values were characterized statistically by the use of eqn (1) and (2) of

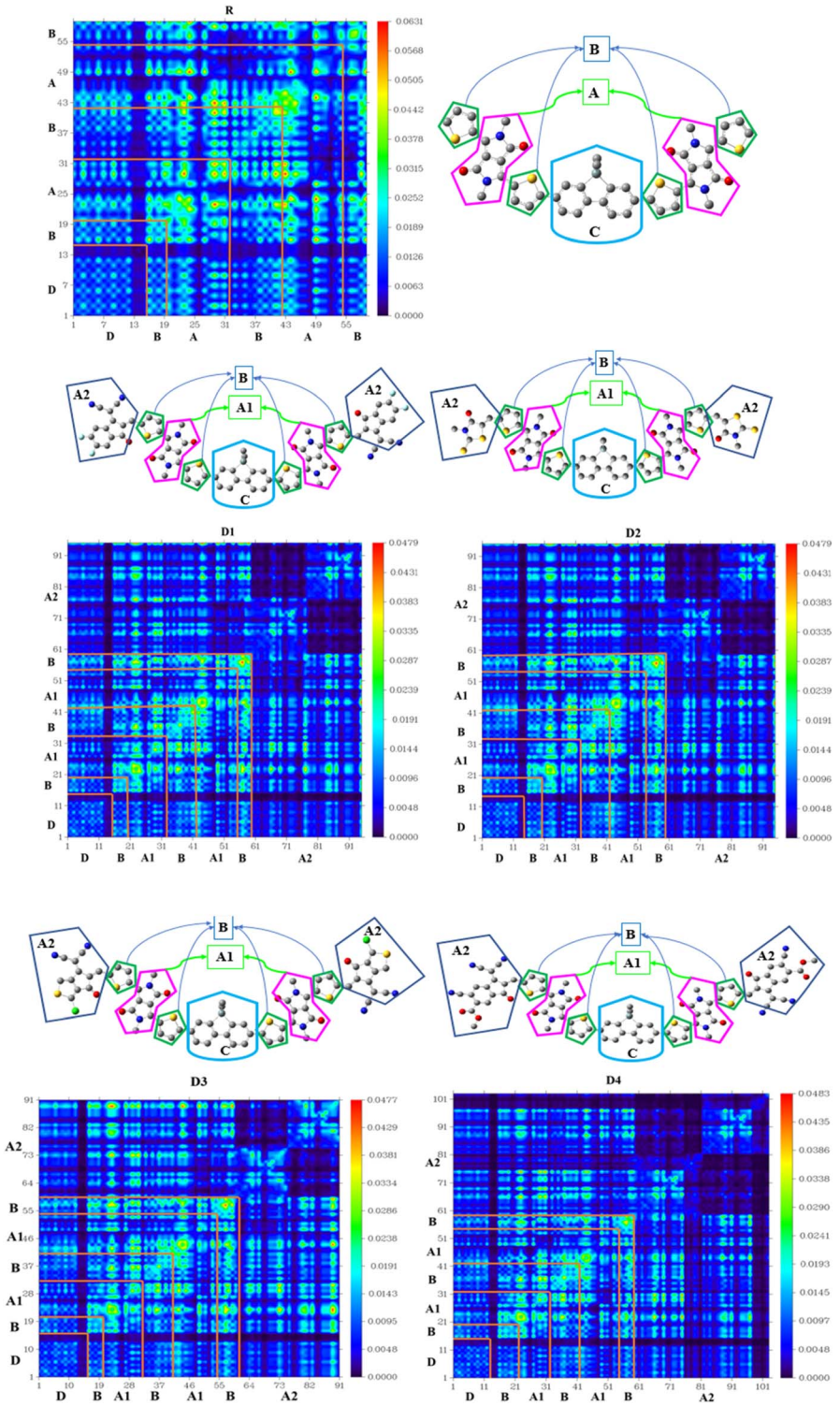

Fig. 8 2-D TDM plots for **R** (DBS-2DPP) and all (**D1–D4**) newly developed molecules.

Marcus theory, which emphasizes the structure of molecules and their stacking arrangement.[60]

Reorganization energy values for electrons (λ_e) and for holes (λ_h) for reference and the architectured molecules (**D1–D4**) are tabulated in Table 6. Attributed to the presence of a powerful electron-pulling moiety, all architectured molecules could have the higher electron and hole mobilities in comparison to the reference. **D1–D4** have computed values of λ_e of 0.12354, 0.14450, 0.11266, and 0.10368 eV, respectively, while reference has a value of 0.15429 eV. Thus, the electron mobility of **D4** seems to be the highest one amongst all, because of the lowest

Table 5 Values of exciton binding energy (E_b) in both the gas phase and DCM solvent for reference and D1–D4 designed molecules

Molecule	E_b gas (eV)	E_b DCM (eV)
R	0.20	0.24
D1	0.19	0.28
D2	0.19	0.26
D3	0.18	0.26
D4	0.15	0.26

Table 6 Reorganization energy values (eV) for electrons (λ_e), as well as for holes (λ_h), for reference and the architectured molecules

Molecule	$\lambda_{e\ (electron)}$	$\lambda_{h\ (hole)}$
R	0.15429	0.17633
D1	0.12354	0.14531
D2	0.14450	0.15266
D3	0.11266	0.14123
D4	0.10368	0.14395

value of λ_e in charge transfer between the donating and accepting components shown by this molecule.

The hole reorganization energy for reference **R** is 0.17933 eV, while other molecules (**D1–D4**) have λ_h values of 0.14531, 0.15266, 0.14123, and 0.14395 eV, correspondingly as provided in (Table 6). Here, the trend followed by the molecules under study for λ_h is **R** > **D2** > **D1** > **D4** > **D3**. So, the highest hole mobility could be **D3** molecule, attributed to its lowest λ_h of all. While, the hole mobility of **D4** might also be a close second to **D3** molecule due to the slight difference in their λ_h.

Concisely, the **D4** molecule might have the highest electron mobility, while the **D3** molecule could have the highest hole mobility among other developed molecules. Thus, both of these developed molecules are thought to be the most effective charge-transporting materials for future applications in solar cells.

3.9. Global reactivity descriptors

To analyze global reactivity indices, some useful measurements for characterizing chemical reactivity and kinetic stability, HOMO–LUMO energy levels, and their difference, *i.e.*, the band-gap, can be utilized. The molecules having narrow band-gaps are more reactive when compared to those which have broader band-gaps and higher stability.[61] Ionization potential and electron affinity are rather important global reactivity indices when evaluating charge carriers' transfer properties in molecules. The higher molecular reactivity of the molecules is associated with high EA values, and their higher stability is related to high IP values. The values of both the studied reactivity indices were calculated using eqn (5) and (6), shown below, and are presented in Table 7.

$$\mathrm{IP} = (E_+ - E_0) \quad (5)$$

$$\mathrm{EA} = (E_0 - E_-) \quad (6)$$

Table 7 Table representing the calculated IP and EA values of all the evaluated chromophores

Molecule	IP (eV)	EA (eV)
R	5.56	1.87
D1	5.89	3.00
D2	5.67	2.53
D3	5.87	3.02
D4	5.99	3.20

A significant connection is seen between ionization potentials and HOMO energies, while electron affinity is shown to be related to LUMO energies. Thus, as a result of the fact that **R** has the greatest HOMO energy of all the molecules investigated, it possesses the lowest IP value and is the least stable molecule. While **D4** has the highest IP value due to its lowest HOMO energy, and thus is the most stable molecule and due to this stability could act proficiently as a donor in the photo-active layer.[62] Similarly, higher values of EA were demonstrated by all newly developed molecules because of their lower LUMO energy levels. EA values for reference and entire designed chromophores are grouped in a descending order as **D4** (3.20) > **D3** (3.02) > **D1** (3.00) > **D2** (2.53) > **R** (1.87), showing their enhanced reactivity than the reference. Even here, **D4** molecule seems to be an effective chromophore, attributed to its highest reactivity, while retaining its stability as well (Fig. 9).

3.10. Dipole moments

The solubility, dipole moment, and charge mobility of organic molecules are all interrelated to one another. A molecule with a high value of dipole moment tends to be highly soluble in a polar organic solvent due to the high degree of charge mobility in it.[63] The increased dipole moments cause the respective molecules to easily self-assemble in a packed and antiparallel orientation, which results in an increased charge transfer rate at the active-layer.[64] A smooth surface of the donor–acceptor interface of the active layer enables the molecule to be readily

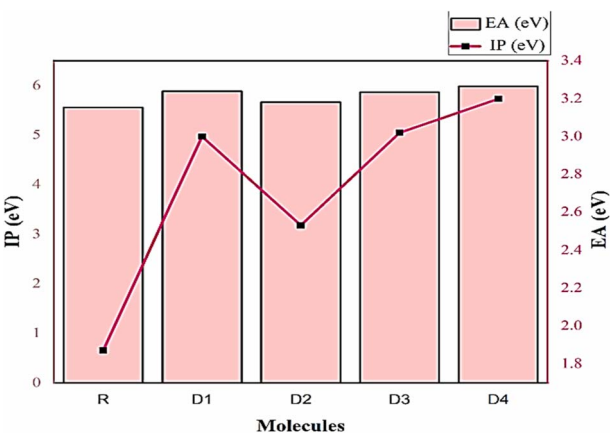

Fig. 9 Global reactivity descriptors (IP and EA) plot for R and all newly developed molecules.

dissolved, resulting in a more efficient solar device assembly.[65] With the help of the information attained about the solubility, polarization, and crystallinity of any molecule, attained from its dipole moment value, its utilization in the solution processing techniques for the construction of OPVs can be made possible. Planarity plays a contributing role in enhancing or diminishing the dipole moment of a molecule. Generally, the planar and organized geometries of molecules with increased dipole moments result in a tighter molecular assembly, improved crystallinity, and higher solubility in polar solvent. But, in a highly planar molecule due to the cancellation of opposite charges within its structure, the dipole moment is generally quite lowered.[66] The values of dipole moments in the gas phase, as well as DCM solvent, are summarized in Table 8. In the gas medium, the dipole moment is following the declining order of **D4** (11.73 D) > **D1** (7.16 D) > **D3** (6.51 D) > **D2** (2.36 D) > **R** (0.83 D), while **D4** (14.75 D) > **D1** (8.80 D) > **D3** (8.13 D) > **D2** (3.45 D) > **R** (1.09 D) is the observed trend of molecules in DCM, as seen in Fig. 10. As a result of these findings, dipole moments in the gaseous and solvent states are found to be significantly higher than that of the reference's value. In dichloromethane, all proposed SMs were shown to have a superior solubility effect than **R**, since their π-interactions in the polar DCM solvent are stronger.

3.11. Molecular electrostatic potential surface (MEPS)

The probable charge transfer passage among donor, bridges, and acceptor moieties at the ground state was measured using the molecular electrostatic potential surface (MEPS) maps.[63] The electrophilic and nucleophilic regions of the molecules under investigation were found *via* the use of MEPS simulations run at the designated DFT functional.[67] In the red zones of the MEPS plots, a negative electrostatic potential, because of the excess of electrons is predicted. While in the blue zones, the opposite seems to be true, due to the deficiency of electrons and thus positive electrostatic potential of those areas. In addition, the green colored regions indicate the presence of the neutral sites. As the red regions have high negative surface potential, they are predicted to be zones for any electrophilic attack, while the blues zone, due to their high positive potential, are susceptible to attack by an incoming nucleophile. For easier understanding, the observed order of electrostatic potential from colored bar of Fig. 11 is written as; red > green > yellow > blue, shifting from negative to positive maxima.

There are quite plenty of red and yellow patches dispersed within the blue donor region on the MEPS of the reference molecule, suggesting the relatively indistinguishable electrophilic and nucleophilic attacking sites in it. Although, the terminal unsaturated oxygen atoms of the reference molecule are bright red zones of nucleophilic attack, just like the unsaturated nitrogen and oxygen atoms of the derived molecules. But in the derived molecules, there are distinct red zones at the peripheral acceptor regions, and blue zones at the rest of the molecule. The majority of blue regions in the derived chromophores point towards their better aptitude as donors with their positive potential in the active layer. The majority of blue regions in the derived chromophores point towards their better aptitude as donors with their positive potential in the active layer. The maximum condensed red patches at the peripheries of the **D4** molecule could be due to its significantly conjugated and electron withdrawing added acceptor group.[39]

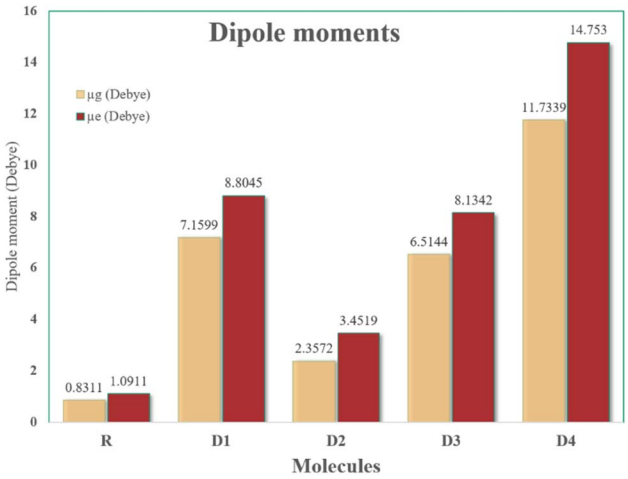

Fig. 10 Colored plot of dipole moments (μ_g along with μ_e) of newly devised D1–D4 as well as R molecules.

Table 8 Dipole moment values of R as well as newly developed D1–D4 in both gaseous and DCM mediums

Molecules	μ_g (Debye)	μ_e (Debye)
R	0.8311	1.0911
D1	7.1599	8.8045
D2	2.3572	3.4519
D3	6.5144	8.1342
D4	11.7339	14.7530

3.12. Device efficiency

The open circuit photo-voltage, fill factor, and short circuit current density of any chromophore, are all important factors in determining the overall performance of the corresponding solar cell.

Open circuit photo-voltage (V_{OC}). When there is no external pressure placed on optical materials, their ability to generate a substantial amount of voltage accurately represents their potential. While estimating PCE of OSCs, open circuit photo-voltage (V_{OC}) is amongst the most significant components to contemplate. It is feasible to determine the photovoltaic efficiency of a solar device by measuring the photo-voltage generated with its open circuit.[68] In addition, an increase in open circuit photo-voltage (V_{OC}) results in an increase in fill factor, which serves as the basis for solar cells' high effectiveness.

The maximum open circuit photo-voltage that may be generated by a SC (due to the photoelectric effect) is governed by intensity of incident light, charge mobility, temperature of device, and the FMOs of the donor and acceptor molecules at the photo-active layer. Here, the V_{OC} of the considered donors was calculated by taking a theoretically proficient and effective

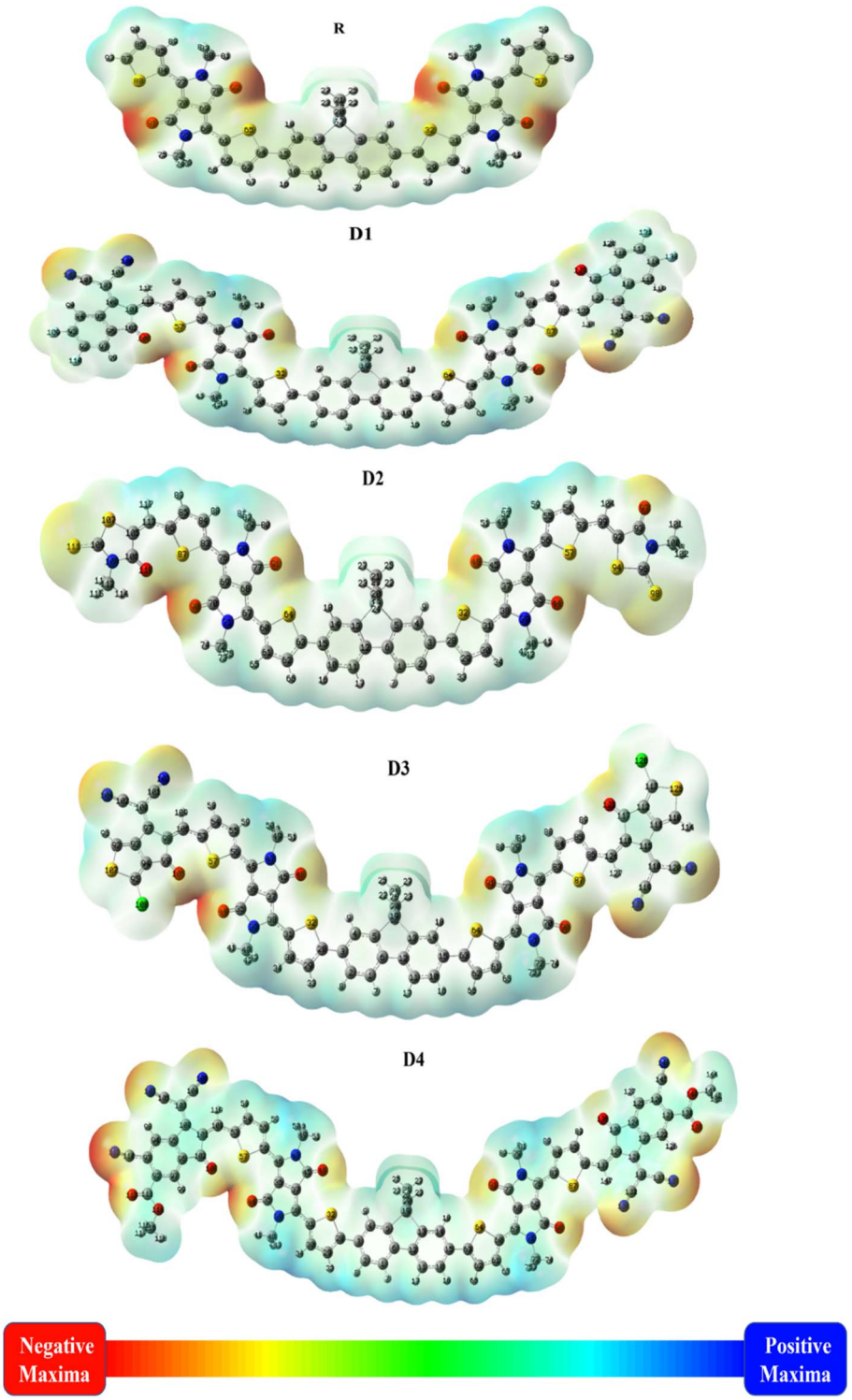

Fig. 11 Molecular electrostatic potential surface (MEPS) colored maps of newly devised **D1–D4** molecules, along with **R**.

acceptor; $PC_{61}BM$.[69] The selected acceptor, with a HOMO of −6.3 eV and LUMO of −3.7 eV, has been known to be a powerful fullerene acceptor and provides acceptable efficiency for the respective solar cells. The reason behind the selection of our proposed molecules to be donors is the fact that a high value of V_{OC} is achievable by lowering the energy level of HOMO in donor material and increasing the energy levels of LUMO in acceptor material of the photo-active layer.[70] So, because of their low HOMO level than reference, all of the derived chromophores are predicted to have improved charge conduction and function as donor materials.

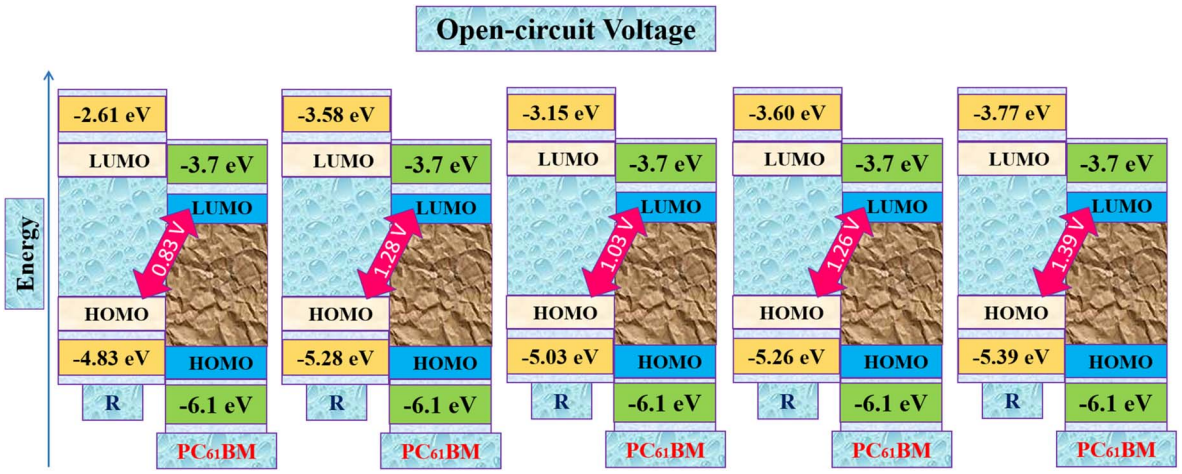

Fig. 12 V_{OC} of proposed compounds, as well as the reference molecule, calculated using $PC_{61}BM$ as the acceptor.

Actually, the open circuit photo-voltage (V_{OC}) was obtained by subtracting the studied donors' HOMO from the acceptor's LUMO and dividing it with the charge of the molecule (taken as 1). In addition, a value of 0.3 was also subtracted as a common empirical value in fullerene acceptor based solar cells.[71] Eqn (7) mathematically represents the relation stated above ,[66] and the thus attained values are represented pictorially in Fig. 12.

$$V_{OC} = \frac{E_{LUMO\ of\ acceptor} - E_{HOMO\ of\ donor}}{e} - 0.3 \quad (7)$$

The voltaic strength of reference and designed compounds studied in terms of V_{OC} rises in the trend as; **R** (0.83 V) < **D2** (1.03 V) < **D3** (1.26 V) < **D1** (1.28 V) < **D4** (1.39 V). From these values, it seems that all the newly proposed compounds could act as better donor materials in the photo-active layer of SC than reference. Among the proposed molecules, **D4** retained its position as the best amongst all due to its relatively higher V_{OC} than all others in the group. Specifically, with the highly electron-withdrawing cyano and acetyl groups of the added end-capped acceptor stabilizing its HOMO value, **D4** has the greatest V_{OC} value of any molecule.

Fill factor (FF). When evaluating the PCE of solar power systems, one of the most important factors to consider is the fill factor (or the amount of energy that is converted).[72] Despite its intricacy, the V_{OC} of the donor–acceptor contact makes it easy to calculate the theoretically estimated value of FF and has a significant impact on it as well. Eqn (8) has been used to determine FF mathematically.[73,74]

$$FF = \frac{\frac{eV_{OC}}{K_BT} - \ln\left(\frac{eV_{OC}}{K_BT} + 0.72\right)}{\frac{eV_{OC}}{K_BT} + 1} \quad (8)$$

In this equation, K_B represents the Boltzmann constant and T represents the temperature in Kelvin of $8.61733034 \times 10^{-5}$ eV and 300 K, respectively. While the whole term eV_{OC}/K_BT is collectively represented as the normalized V_{OC}.[75] Table 9 presents a summary of the theoretical findings of the normalized V_{OC} and FF. FF of all developed molecules is in the same order as V_{OC}. So, upon comparison, it was evaluated that all the newly synthesized **D1–D4** chromophores have higher FF than reference, with **D4** having the highest one amongst all. The increment in the FF of newly constructed molecules proves their better efficacy than the reference, and thus they could be more effective in the photo-active layer of OPVs.

Power conversion efficiency (PCE). The PCE of a solar cell is used to consolidate all of the above-calculated output data into a single value, to determine the ultimate effectiveness of the corresponding solar cell for practical use. The following is eqn (9) for calculating PCE.[73]

$$PCE = \frac{J_{SC}V_{OC}FF}{P_{in}} \quad (9)$$

Here, the power of incident photons on solar cells is P_{in}, and typically during the theoretical calculations of PCE, this P_{in} is set at AM 1.5G and 100 mW cm^2. From this equation, it is elaborated that FF, V_{OC}, and short circuit current density (J_{SC}) have a direct impact on PCE values. The values of FF and V_{OC} of all the newly formulated molecules were higher than the reference molecule, making them out to be better contenders in solar cells. Furthermore, while the J_{SC} value was not calculated in this study, eqn (10) below illustrates its direct relation with the LHE.

Table 9 Values of normalized V_{OC} and FF of the R, as well as D1–D4 designed molecules

Molecule	Normalized V_{OC} $\left(\frac{eV_{OC}}{K_BT}\right)$	Fill factor
R	32.11	0.864
D1	49.51	0.903
D2	39.84	0.885
D3	48.74	0.901
D4	53.77	0.909

$$J_{SC} = \left[\int_{\lambda}^{0} \mathrm{LHE}(\lambda)(\phi_{\mathrm{injected}})(\eta_{\mathrm{collected}})\mathrm{d}\lambda\right] \quad (10)$$

Here, $\varphi_{\mathrm{injected}}$ represents the efficiency of injection of electrons, while $\eta_{\mathrm{collected}}$ denotes the efficiency of charge collection. As the newly designed chromophores had better LHE than reference in both the gas phase and DCM solvent, they are supposed to have higher short-circuit current density as well. Thus attributed to the above-studied parameters, all of the newly proposed molecules could have higher PCE than the reference.

4. Conclusion

In this investigation, four A_2–π–A_1–π–D–π–A_1–π–A_2 type small-molecule donors were theoretically designed and explored under DFT, in order to possibly improve the photovoltaic properties and efficiency of OSCs. Here, a dibenzosilole-based DBS-2DPP molecule was taken as the reference and four new molecules were developed from it, with the addition of terminal acceptors at its peripheries. These added acceptor groups by shifting the electron density towards themselves, better differentiated the donor and acceptor components of the molecules, helping them in effective charge transport within their structures. Attributed to the A_2 acceptors, the performed quantum chemical computations of the newly proposed molecules were seen to be rather substantially improved when compared to the reference. All of the proposed structures demonstrated extensive absorption in the near IR region in both the studied phases. Their band-gaps, excitation and exciton binding energies, reorganization energies, oscillation strengths and dipole moments all pointed towards their better performance than the reference. The studied FMOs, MEPS, TDM, and DOS analysis also showed the effective charge density distribution in the derived molecules. In addition, their calculated PCE factors with $PC_{61}BM$ acceptor, *i.e.*, open circuit photo-voltage, light harvesting efficiencies, and fill factor, were also transparently boosted. Although all the newly derived chromophores were better than reference in all the studied aspects of solar cells, **D4** seemed to be the best of all. With its highest dihedral angle, SDP, and MPP, this molecule while retaining its planar identity maintained discrete acceptor and donor regions in its structure, which helped it in lowering its exciton binding energy in gas phase (0.15 eV), increasing its dipole moment in both DCM (14.7530 D) and gas (11.7339 D) phase, as well as reducing its required λ_e (0.10368 eV). In addition, attributed to the strongly electron-withdrawing peripheral (A_2) acceptors of **D4**, this molecule had the most highly stabilized FMOs amongst all, due to which it showed the lowest band-gap (1.62 eV), the highest V_{OC} (1.39 V), and the maximum IP and EA of 5.99 and 320 eV, respectively. Most importantly, due to the highly conjugated cyano and acetyl groups in its added acceptor, **D4** demonstrated the highest λ_{max} of 876 nm in DCM and 802 nm in gas phase, and the lowest excitation energies of 1.47 eV in gas phase and 1.36 nm in the DCM solvent. Amongst all the studied parameters, only its binding energy in the solvent phase (0.26 eV), just like other proposed molecules was somewhat inferior to the reference molecule (0.24 eV), but this could be attributed to their enhanced compatibility with the studied solvent. Although **D3** molecule seemed to be a close second to **D4** molecule, due to its studied values being quite adjacent to **D4** with some of them even exceeding it, such as its lowest λ_h, highest oscillator strength, and the highest light harvesting efficiencies. But, it's relatively lowered open circuit photo-voltage and fill factor reduced its aptitude in comparison to **D4**. In short, the strategy of adding new acceptor groups in the reference molecule has provided us with quite effective molecules, with **D4** being the most effective one of all. Thus, all of them could be applied for their possible practical applications in future organic photovoltaic cells.

Conflicts of interest

The authors declare no conflict of interest.

Acknowledgements

The authors acknowledge the technical provided by Department of Chemistry, University of Agriculture (UAF), Faisalabad 38000, Pakistan. The authors extend their appreciation to the Researchers Supporting Project number (RSP-2021/396), King Saud University, Riyadh, Saudi Arabia. The authors also thankful to Dr Khurshid Ayub, COMSATS University, Islamabad, Abbottabad Campus, Pakistan for additional resources.

References

1 W. Fulkerson, R. R. Judkins and M. K. Sanghvi, *Sci. Am.*, 1990, **263**, 128–135.
2 A. M. Omer, *Renew. Sustain. Energy Rev.*, 2008, **12**, 2265–2300.
3 K. Tromly, *Renewable Energy: An Overview*, United States, N. p., 2001.
4 M. Ans, J. Iqbal, I. A. Bhatti and K. Ayub, *RSC Adv.*, 2019, **9**, 34496–34505.
5 A. K. Abdelsalam, H. T. Shahin and I. Morsi, *IEEE Second International Conference on DC Microgrids (ICDCM)*, 2017, pp. 406–414.
6 R. Ma, T. Yang, Y. Xiao, T. Liu, T. Yang, R. Ma, L. Zhan, Z. Luo, G. Zhang and H. Yan, *Joule*, 2021, **5**(4), 914–930.
7 P. Würfel, *Phys. E*, 2002, **14**, 18–26.
8 M. Mrinalini, N. Islavath, S. Prasanthkumar and L. Giribabu, *Chem. Rec.*, 2019, **19**, 661–674.
9 K. J. Yu, Z. Yan, M. Han and J. A. Rogers, *npj Flexible Electron.*, 2017, **1**(1), 1–14.
10 Q. Tan, X. Yang, M. Cheng, H. Wang, X. Wang and L. Sun, *J. Phys. Chem. C*, 2014, **118**, 16851–16855.
11 Y. Xu, F. Zhang and X. Feng, *Small*, 2011, **7**, 1338–1360.
12 R. Saleem, A. Farhat, R. A. Khera, P. Langer and J. Iqbal, *Comput. Theor. Chem.*, 2021, **1197**, 113154.
13 M. Ans, K. Ayub, I. A. Bhatti and J. Iqbal, *RSC Adv.*, 2019, **9**, 3605–3617.
14 Y. Lin and X. Zhan, *Mater. Horiz.*, 2014, **1**, 470–488.
15 B. Walker, J. Liu, C. Kim, G. C. Welch, J. K. Park, J. Lin, P. Zalar, C. M. Proctor, J. H. Seo and G. C. Bazan, *Energy Environ. Sci.*, 2013, **6**, 952–962.

16 W. Li, K. H. Hendriks, M. M. Wienk and R. A. Janssen, *Acc. Chem. Res.*, 2016, **49**, 78–85.
17 Y. Lin, Y. Li and X. Zhan, *Adv. Energy Mater.*, 2013, **3**, 724–728.
18 S. J. Akram, N. Hadia, J. Iqbal, R. F. Mehmood, S. Iqbal, A. M. Shawky, A. Asif, H. Somaily, M. Raheel and R. A. Khera, *RSC Adv.*, 2022, **12**, 20792–20806.
19 F. Ogliaro, M. Bearpark, J. Heyd, E. Brothers, K. Kudin, V. Staroverov, R. Kobayashi, J. Normand, K. Raghavachari, A. Rendell and D. J. Fox, *Gaussian 09, revision a. 02.*, Gaussian., Inc., Wallingford, CT, 2009.
20 S. J. Akram, J. Iqbal, M. Ans, Y. A. El-Badry, R. F. Mehmood and R. A. Khera, *Sol. Energy*, 2022, **237**, 108–121.
21 R. D. I. I. Dennington, T. A. Keith and J. M. Millam, *GaussView, version 6.0. 16.*, Semichem Inc Shawnee Mission KS., 2016.
22 J. P. Finley, *Mol. Phys.*, 2004, **102**, 627–639.
23 A. Alparone, *Chem. Phys. Lett.*, 2013, **563**, 88–92.
24 C. Adamo and V. Barone, *J. Chem. Phys.*, 1998, **108**, 664–675.
25 J.-D. Chai and M. Head-Gordon, *Phys. Chem. Chem. Phys.*, 2008, **10**, 6615–6620.
26 J. Zhang, H.-B. Li, S.-L. Sun, Y. Geng, Y. Wu and Z.-M. Su, *J. Mater. Chem.*, 2012, **22**, 568–576.
27 M. Cossi, V. Barone, B. Mennucci and J. Tomasi, *Chem. Phys. Lett.*, 1998, **286**, 253–260.
28 L. A. Deschenes and A. David Vanden Bout, University of Texas, 2000.
29 T. Lu, *J. Mol. Model.*, 2021, **27**, 1–6.
30 T. Lu and F. Chen, *J. Comput. Chem.*, 2012, **33**, 580–592.
31 W. Humphrey, A. Dalke and K. Schulten, *J. Mol. Graph.*, 1996, **14**, 33–38.
32 A. Tenderholt, in Stanford University, CA Stanford, 2006.
33 S. J. Akram, J. Iqbal, R. F. Mehmood, S. Iqbal, Y. A. El-Badry, M. I. Khan, M. Ans and R. A. Khera, *Sol. Energy*, 2022, **240**, 38–56.
34 T. Tani, T. Suzumoto and K. Ohzeki, *J. Phys. Chem.*, 1990, **94**, 1298–1301.
35 I. Bahar, M. Kaplan and R. Jernigan, *Proteins: Struct., Funct., Bioinf.*, 1997, **29**, 292–308.
36 M. Khalid, A. Ali, R. Jawaria, M. A. Asghar, S. Asim, M. U. Khan, R. Hussain, M. F. ur Rehman, C. J. Ennis and M. S. Akram, *RSC Adv.*, 2020, **10**, 22273–22283.
37 S. Zahid, A. Rasool, M. Ans, M. Yaseen and J. Iqbal, *Energy Fuels*, 2021, **35**, 15018–15032.
38 M. Rafiq, M. Salim, S. Noreen, R. A. Khera, S. Noor, U. Yaqoob and J. Iqbal, *J. Mol. Liq.*, 2022, **345**, 118138.
39 M. I. Khan, J. Iqbal, S. J. Akram, Y. A. El-Badry, M. Yaseen and R. A. Khera, *J. Mol. Graph. Model.*, 2022, **113**, 108162.
40 A. Naveed, R. A. Khera, U. Azeem, I. Zubair, A. Farhat, A. R. Ayub and J. Iqbal, *Mater. Sci. Semicond. Process.*, 2022, **137**, 106150.
41 M. Salim, M. Rafiq, R. A. Khera, M. Arshad and J. Iqbal, *Sol. Energy*, 2022, **233**, 31–45.
42 M. U. Saeed, J. Iqbal, R. F. Mehmood, S. J. Akram, Y. A. El-Badry, S. Noor and R. A. Khera, *Surface. Interfac.*, 2022, **30**, 101875.
43 U. Mubashar, A. Farhat, R. A. Khera, N. Iqbal, R. Saleem and J. Iqbal, *J. Mol. Model.*, 2021, **27**, 1–13.
44 R. A. Shehzad, J. Iqbal, M. U. Khan, R. Hussain, H. M. A. Javed, A. ur Rehman, M. U. Alvi and M. Khalid, *Comput. Theor. Chem.*, 2020, **1181**, 112833.
45 A. Rasool, S. Zahid, R. A. Shehzad, M. S. Akhter and J. Iqbal, *Comput. Theor. Chem.*, 2021, **1203**, 113359.
46 M. Miar, A. Shiroudi, K. Pourshamsian, A. R. Oliaey and F. Hatamjafari, *J. Chem. Res.*, 2021, **45**, 147–158.
47 T. Liu, Y. Zhang, Y. Shao, R. Ma, Z. Luo, Y. Xiao, T. Yang, X. Lu, Z. Yuan and H. Yan, *Adv. Funct. Mater.*, 2020, **30**, 2000456.
48 Z. Luo, R. Ma, T. Liu, J. Yu, Y. Xiao, R. Sun, G. Xie, J. Yuan, Y. Chen and K. Chen, *Joule*, 2020, **4**, 1236–1247.
49 M. Ans, J. Iqbal, B. Eliasson and K. Ayub, *Comput. Mater. Sci.*, 2019, **159**, 150–159.
50 I. Zubair, R. A. Kher, S. J. Akram, Y. A. El-Badry, M. U. Saeed and J. Iqbal, *Chem. Phys. Lett.*, 2022, **793**, 139459.
51 S. Tretiak and S. Mukamel, *Chem. Rev.*, 2002, **102**, 3171–3212.
52 S. Anwar, N. Naeem, Z. M. Elqahtani, S. Siddique, J. Iqbal, M. Al-Buriahi and S. Alomairy, *Chem. Phys. Lett.*, 2022, 139726.
53 M. Ans, J. Iqbal, B. Eliasson, M. J. Saif, H. M. A. Javed and K. Ayub, *J. Mol. Model.*, 2019, **25**, 1–12.
54 L. Bhattacharya, S. Sharma and S. Sahu, *Int. J. Quantum Chem.*, 2021, **121**, e26524.
55 K. Q. Kayani, U. Yaqoob, S. Jabeen, S. Iqbal, M. Yaseen, M. Khalid, M. S. Akhter and J. Iqbal, *Comput. Theor. Chem.*, 2021, **1202**, 113305.
56 M. Schapira, M. Totrov and R. Abagyan, *J. Mol. Recognit.*, 1999, **12**, 177–190.
57 A. Rasool, S. Zahid, M. Ans, S. Muhammad, K. Ayub and J. Iqbal, *ACS Omega*, 2021, **7**(1), 844–862.
58 M. Ans, K. Ayub, X. Xiao and J. Iqbal, *J. Mol. Liq.*, 2020, **298**, 111963.
59 S. A. Siddique, M. B. A. Siddique, R. Hussain, X. Liu, M. Y. Mehboob, Z. Irshad and M. Adnan, *Comput. Theor. Chem.*, 2020, **1191**, 113045.
60 I. Yousaf, R. A. Khera, J. Iqbal, S. Gul, S. Jabeen, A. Ihsan and K. Ayub, *Mater. Sci. Semicond. Process.*, 2021, **121**, 105345.
61 A. Musawwir, A. Farhat, R. A. Khera, A. R. Ayub and J. Iqbal, *Comput. Theor. Chem.*, 2021, **1201**, 113271.
62 A. Naveed, S. J. Akram, M. Ans, J. Iqbal, I. Batool, R. F. Mehmood and R. A. Khera, *J. Mol. Model.*, 2022, **28**, 1–16.
63 U. Azeem, R. A. Khera, A. Naveed, M. Imran, M. A. Assiri, M. Khalid and J. Iqbal, *ACS Omega*, 2021, **6**, 28923–28935.
64 U. Yaqoob, S. Rafiq, S. U. Rehman, S. Bibi and J. Iqbal, *Optik*, 2021, **246**, 167845.
65 L. Lu, T. Zheng, Q. Wu, A. M. Schneider, D. Zhao and L. Yu, *Chem. Rev.*, 2015, **115**, 12666–12731.
66 M. U. Saeed, J. Iqbal, R. F. Mehmood, M. Riaz, S. J. Akram, H. Somaily, A. M. Shawky, M. Raheel, M. I. Khan and E. U. Rashid, *J. Phys. Chem. Solids*, 2022, **170**, 110906.
67 J. S. Puranen, M. J. Vainio and M. S. Johnson, *J. Comput. Chem.*, 2010, **31**, 1722–1732.

68 D. Credgington and J. R. Durrant, *J. Phys. Chem. Lett.*, 2012, **3**, 1465–1478.
69 D. Chirvase, Z. Chiguvare, M. Knipper, J. Parisi, V. Dyakonov and J. C. Hummelen, *J. Appl. Phys.*, 2003, **93**, 3376–3383.
70 M. Ans, J. Iqbal, Z. Ahmad, S. Muhammad, R. Hussain, B. Eliasson and K. Ayub, *ChemistrySelect*, 2018, **3**, 12797–12804.
71 M.-H. Lee, *Sol. Energy*, 2022, **234**, 360–367.
72 A. Farhat, R. A. Khera, S. Iqbal and J. Iqbal, *Opt. Mater.*, 2020, **107**, 110154.
73 U. Yaqoob, A. R. Ayub, S. Rafiq, M. Khalid, Y. A. El-Badry, Z. M. El-Bahy and J. Iqbal, *J. Mol. Liq.*, 2021, **341**, 117428.
74 L. Zhang, W. Shen, R. He, X. Liu, X. Tang, Y. Yang and M. Li, *Org. Electron.*, 2016, **32**, 134–144.
75 M. Rafiq, R. A. Khera, M. Salim, M. Khalid, K. Ayub and J. Iqbal, *Chem. Phys. Lett.*, 2021, **782**, 139018.